Hindawi
Geofluids
Volume 2022, Article ID 3282276, 14 pages
https://doi.org/10.1155/2022/3282276

Research Article

Research on the Identification of Precursor Information of Limestone Rockburst under Triaxial Unloading Conditions

Wenjun Ding, Zonghong Zhou, Jian Liu, Tingkai Hou, Jiaxin Wang, Jin Li, and Xin Zhang

Faculty of Land Resources Engineering, Kunming University of Science and Technology, Kunming 650093, China

Correspondence should be addressed to Zonghong Zhou; zhouzh@kmust.edu.cn

Received 8 July 2021; Revised 5 October 2021; Accepted 23 October 2021; Published 16 March 2022

Academic Editor: Xudong Zhang

Based on the energy evolution of limestone and acoustic emission evolution law, this paper takes the limestone unloading energy evolution law and acoustic emission cumulative ringing count, cumulative energy, RA value, acoustic emission information entropy, and acoustic emission damage as precursor discrimination indicators for the occurrence of rock explosion. Study of the impact of the unloading rate on the rock explosion precursors indicates that with increasing unloading rate there are more dramatic changes in the degree of each precursor discrimination indicators and rock ruptures within a short period of time before the completion of the indicators. The establishment of the precursor response coefficient reveals that the precursor response is the strongest when the rock rupture acoustic emission RA value time is the earliest. The remaining four precursor discrimination indicators of rock rupture with different loading paths show fluctuations in the identification capacity of the state. The research results can provide some reference for identifying rockburst precursor information.

1. Introduction

Rockburst is a dynamic phenomenon in which the elastic variable situation energy accumulated in the underground engineering rock is suddenly released under excavation or other external disturbances, resulting in the bursting and ejection of the surrounding rock [1]. As mining activities gradually move to deeper areas, mines are often faced with a series of problems such as increased rock stress and increased ground temperature. Among them, rockburst is the most difficult to deal with [2]. Papadopoulos and Benardos [3] used machine learning (ML) to predict rockbursts. The evaluation results showed that SMOTE had a tremendous positive effect in improving the accuracy of classification within the class. Zhang et al. [4] established rockburst predictions based on tunnel engineering data. He et al. [5] comprehensively considered the strength ratio and friction of rock materials and proposed a new method for on-site prediction of rockburst tendency of rock materials. Khan et al. [6] introduced a new method of drawing induced fissures and related line graphs based on microseismic data to identify and predict dangerous areas that may lead to coal mine collapse or rockburst. Zhang et al. [7] used the experimental results and numerical simulation analysis of Hopkinson pressure bar (SHPB) to discuss the energy mechanism of coal and gas outburst induced by rockburst. Su et al. [8] used the true triaxial rockburst test system to obtain the static period, waveform fractal dimension, and activity of MS significant characteristics such as level, B value, and frequency spectrum. Based on the unified strength theory (UST), Jing-Lin et al. [9] established a rockburst instability model and analyzed the intermediate principal stress (IPS) and coal seam strength parameters (the influence of cohesion and internal friction angle) on the distribution characteristics of rockburst. Jia et al. [10] used numerical simulation methods and similar material simulation tests to propose rockburst monitoring methods and prevention measures to effectively reduce the probability of rockburst occurrence. For rockburst monitoring by acoustic emission and rock energy, Su et al. [11] conducted rockburst tests on six intact hard and brittle rock specimens and then investigated rockbursts of different rocks using high-speed

Table 1: Mechanical parameters of limestone.

Rock type	Compressive strength/MPa	Tensile strength/MPa	Modulus of elasticity/GPa	Poisson's ratio
Limestone	65.7	3.62	15.3	0.25
Limestone	57.1	3.25	15.7	0.23
Limestone	59.6	3.62	16.0	0.25

The parameters obtained from the three experiments were averaged to obtain uniaxial compressive strength of 60.8 MPa, tensile strength of 3.50 MPa, modulus of elasticity of 15.67 MPa, and Poisson's ratio of 0.24 for the limestone.

cameras, acoustic emission systems, and scanning electron microscopy. Guo et al. [12] conducted three-point bending tests on prefabricated notched semicircular medium-grained granite specimens and used acoustic emission to monitor the development of microcracks. Tao et al. [13] further investigated the differences in energy decomposition and acoustic emission characteristics during sandstone damage by testing the acoustic emission characteristics of rock specimens under different unloading envelope pressures.

Gao et al. [14] conducted uniaxial compression experiments on five rocks in multiple cycles and analyzed the acoustic emission activities and damage modes of the five rock destruction stages. On this basis, Gao et al. further analyzed the rockburst potential according to the energy conservation index. Jiaxu et al. [15] conducted uniaxial compression tests on amphibolite and recorded the acoustic emission signals to analyze the relationship between various key signals. Mei et al. [16] analyzed the spectral characteristics and time-domain dominant frequency of acoustic emission during the whole rockburst process based on the uniaxial strained rockburst test of deeply buried marble. Wang et al. [17] studied the multiparameter synergistic method for rockburst prediction by true triaxial test.

The current research on rockburst mainly focuses on the definition, classification, research methods, characteristics, formation conditions, prediction methods, and prevention measures of rockburst [18]. The research results of rockburst are quite abundant, and important progress in the mechanism and prediction of rockburst has been made in theory, but there is still a lack of reliable technology for accurate prediction of rockbursts. It is necessary to accurately monitor the process of rock mass energy accumulation, evolution, rock mass rupture, damage, and energy dynamic release during deep mining [19].

This paper studies the precursor laws of rockburst from the perspective of energy and acoustic emission. In terms of energy, the principle of energy calculation is explained, the "energy pressure drop response ratio" is introduced, and the law of energy evolution and energy pressure drop response ratio of limestone under triaxial loading and unloading conditions is analyzed. Based on the energy evolution law, a rockburst is proposed. The change characteristics of the response ratio of energy and energy pressure drop of the rock sample before life (i.e., rockburst precursor information), the total energy, elastic energy, dissipated energy, axial strain energy, and hoop strain energy with the confining pressure and the changing law of unloading rate, the influence of confining pressure, and unloading rate on the information of rockburst precursors are studied. In terms of acoustic emission, the time domain parameters of the rock, including (cumulative) ringing count, (cumulative) acoustic emission energy, and RA value change characteristics, during loading and unloading are studied. The concept of information entropy in thermodynamics is introduced, and the acoustic emission ringing count is calculated. The information entropy is used to quantitatively characterize the failure process of limestone through information entropy. The damage variable of the acoustic emission ringing count is calculated, and the rock failure precursor is studied from the perspective of rock damage evolution. The abovementioned rock fracture precursor identification indicators are selected to construct a multiple precursor information identification systems of acoustic emission time-domain parameters, and a comprehensive analysis of the precursor information of rockburst acoustic emission is carried out.

2. Materials and Methods

The material used in this experiment is limestone, and the rock mechanical parameters are shown in Table 1 [20].

2.1. Energy Calculation Principle. The total strain energy U of the specimen is

$$U = U_1 + U_3, \tag{1}$$

where U_1 is the strain energy absorbed σ_1 by the axial compression and U_3 is the strain energy generated σ_3 by the unloading of the surrounding pressure.

At any moment t in the test process, the absorbed axial strain energy U_1 and the strain energy U_3 consumed by the negative work of the enclosing pressure can be obtained by integrating the stress-strain curve as follows:

$$\begin{cases} U_1 = \int_0^{\varepsilon_1^t} \sigma_1 d\varepsilon_1 = \sum_{t=1}^{n} \frac{1}{2}\left(\sigma_1^t + \sigma_1^{t+1}\right)\left(\varepsilon_1^{t+1} - \varepsilon_1^t\right), \\ U_3 = \int_0^{\varepsilon_3^t} \sigma_3 d\varepsilon_3 = \sum_{t=1}^{n} \left(\sigma_3^t + \sigma_3^{t+1}\right)\left(\varepsilon_3^{t+1} - \varepsilon_3^t\right), \end{cases} \tag{2}$$

where ε_1^t is the axial strain at any point t of the stress-strain curve. ε_3^t is the circumferential strain at any point t in the stress-strain curve, and σ_1^t end σ_3^t are the axial stress and circumferential stress at any point in the stress-strain curve.

Therefore, dissipated energy U_d:

$$U_d = U_1 + U_3 - U_e. \tag{3}$$

2.2. Energy Pressure Drop Response Ratio. In the process of

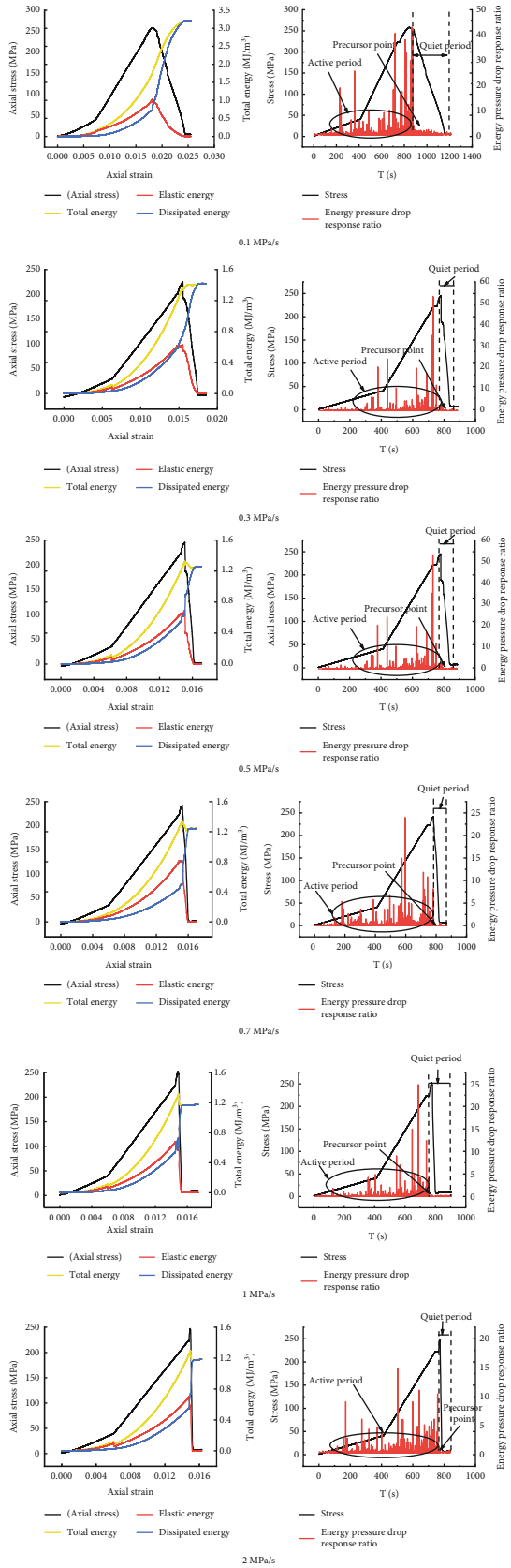

FIGURE 1: Limestone energy and energy pressure drop response ratio under different unloading rates at the same confining pressure (40 MPa).

Table 2: Strain energy density at the peak point.

Unloading rate MPa/s	U_1 MJ/m^3	U_3 MJ/m^3	U_e MJ/m^3	U_d MJ/m^3	U MJ/m^3	U_d/U
0.1	1.7336	0.0279	0.7270	1.0346	1.7616	0.5873
0.3	1.3798	0.0107	0.7545	0.6145	1.3690	0.4489
0.5	1.3285	0.0074	0.6939	0.6273	1.3211	0.4748
0.7	1.3463	0.0138	0.7343	0.5982	1.3325	0.4489
1.0	1.3012	0.0103	0.7261	0.5648	1.2909	0.4375
2.0	1.3068	0.0094	0.7226	0.5748	1.2985	0.4426

Table 3: Strain energy density at the residual point.

Unloading rate MPa/s	U_1 MJ/m^3	U_3 MJ/m^3	U_e MJ/m^3	U_d MJ/m^3	U MJ/m^3	U_d/U
0.1	1.6580	0.2604	0.0003	1.39711	1.3974	0.9999
0.3	1.6446	0.2263	0.0002	1.4181	1.4183	0.9998
0.5	1.4811	0.2242	0.0006	1.2563	1.2570	0.9994
0.7	1.4694	0.2267	0.0006	1.2421	1.2427	0.9995
1.0	1.3861	0.2115	0.0010	1.1736	1.1746	0.9991
2.0	1.3695	0.1820	0.0008	1.1867	1.1875	0.9993

Table 4: Strain energy density at the unloading point.

Unloading rate MPa/s	U_1 MJ/m^3	U_3 MJ/m^3	U_e MJ/m^3	U_d MJ/m^3	U MJ/m^3	U_d/U
0.1	1.3015	0.0094	0.5113	0.7996	1.3109	0.6070
0.3	1.2111	0.0072	0.5822	0.6216	1.2039	0.5163
0.5	1.2080	0.0052	0.5491	0.6537	1.2028	0.5435
0.7	1.2550	0.0065	0.6311	0.6174	1.2485	0.4945
1.0	1.2150	0.0037	0.5341	0.6772	1.2113	0.5591
2.0	1.2454	0.0054	0.5452	0.6959	1.2410	0.5608

unloading test, due to the influence of axial pressure and surrounding pressure, the internal energy evolution of the rock will have a certain influence. From the perspective of the main stress difference, the energy pressure drop response ratio index analyzes the law of the internal energy of the rock with the fast and slow change of axial pressure and surrounding pressure, which can be a good measure of the degree of influence of pressure changes on the deformation, damage, and destruction of the rock in the process of unloading [21].

The energy pressure drop response ratio expression is

$$\frac{\Delta U_{i(t+1)}}{\Delta \sigma_{13(t+1)}} = \frac{U_{i(t+1)} - U_{i(t)}}{\left[\sigma_{1(t+1)} - \sigma_{3(t+1)}\right] - \left[\sigma_{1(t)} - \sigma_{3(t)}\right]}, \quad (4)$$

where $\Delta U_{i(t+1)}$ is the increase in total strain energy (including elastic energy and dissipation energy) inside the rock sample at time $(t+1)$; $U_{i(t+1)}$ and $U_{i(t)}$ are the total strain energy (including elastic energy and dissipation energy) inside the rock sample at $t+1$ and t, respectively; $\Delta\sigma_{13(t+1)}$ indicates the pressure drop at $t+1$; $\sigma_{1(t+1)}$ are $\sigma_{1(t)}$, respectively, indicate the axial pressure at $t+1$ and t; and $\sigma_{3(t+1)}$ are $\sigma_{3(t)}$ indicate the confining pressure at $t+1$ and t, respectively.

2.3. Information Entropy. Shannon [22] pointed out that entropy could simplify complex information by quantified representations and measure the determinism of a state information. The evolution of self-organized critical phenomena in limestones during loading can be visualized by the change in the magnitude of the entropy of acoustic emission ringing count information.

The information entropy is

$$H(X(m,\omega,\sigma)) = -\sum_{i=1}^{\omega+m\sigma} P(x_i)\log_{10}P(x_i). \quad (5)$$

2.4. Acoustic Emission Damage Variables. Kachanov [23]

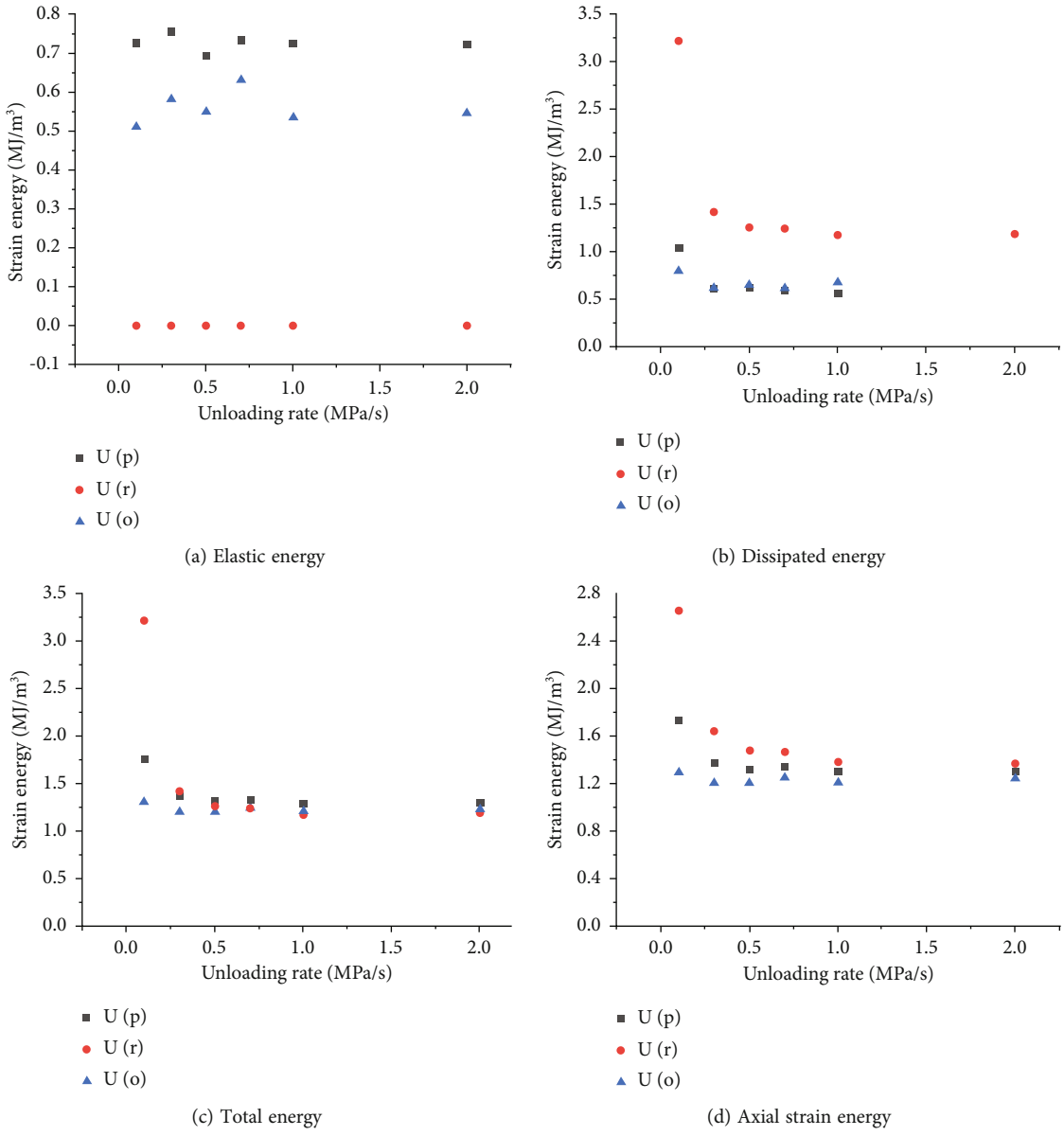

(a) Elastic energy

(b) Dissipated energy

(c) Total energy

(d) Axial strain energy

Figure 2: Continued.

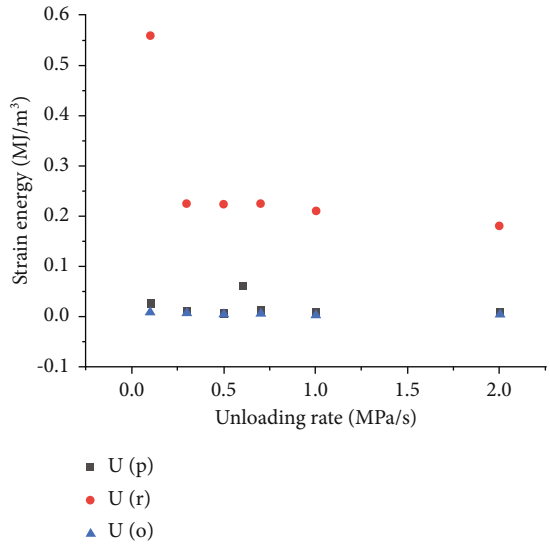

(e) Circumferential strain energy

Figure 2: The relationship between strain energy at unloading point, peak point, and residual point and confining pressure under triaxial loading and unloading conditions. Note: in the figure, p represents the peak point, r represents the residual point, and o represents the unloading point.

Table 5: The time it takes to increase the dissipation energy of the residual stage at different unloading rates.

Unloading rate MPa/s	t/s		
	Peak point	Residual point	Time interval/s
0.1	884	1212	328
0.3	797	948	151
0.5	780	887	107
0.7	780	869	89
1	776	904	128
2	771	840	69

defined the damage variable D as

$$D = \frac{N_t}{N_m}. \tag{6}$$

The range of D is (0, 1), and the larger the value of D, the greater the degree of damage to the rock. When $D = 0$, the rock is not damaged; when $D = 1$, the rock is completely ruptured.

3. Results and Discussion

3.1. Precursor Law of Limestone Energy Evolution under Triaxial Loading and Unloading Conditions. Taking 40 MPa as an example, the response ratio curves of limestone energy and energy pressure drop under the same confining pressure and different unloading rates are shown in Figure 1. At the beginning of loading, the elastic energy of the rock sample is greater than the dissipated energy. When the confining pressure reaches the predetermined value, the confining pressure remains unchanged, and the axial load continues. At this time, the dissipated energy decreases for a short time. This is because the confining pressure remains unchanged and the negative work done by the confining pressure is reduced, resulting in a decrease in the dissipation energy. As the loading continues, the internal cracks in the rock sample begin to initiate, develop, and gradually expand, resulting in a slow rise in the dissipated energy and a gradual decrease in the elastic energy. When the rock sample is loaded to the peak strength, the dissipated energy begins to rise sharply, and the elastic energy drops sharply. Also, the value of the dissipated energy exceeds the elastic energy at that time the rock sample is completely destroyed. Therefore, the rapid changes of the dissipated energy and elastic energy can be used as the precursor information of rockburst caused by the fracture of the rock sample.

The ratio graph shows that the energy pressure drop response of the rock sample is relatively active at the beginning of loading. As the loading continues, the energy pressure drop response ratio continues to be active and the degree of activity increases. It is believed that before the peak strength of the rock sample, the deformation damage of a rock sample is very sensitive to changes in stress. After the peak strength of the rock sample, the energy pressure drop response ratio gradually stabilizes. This is because the sample has been completely destroyed, and the difference between the strain energy and the principal stress simultaneously decreases sharply, resulting in a smaller response ratio of energy pressure drop. Therefore, the energy pressure drop response ratio at the quiet period can be used as the precursor information of the rockburst caused by the failure of the rock sample. When it changes from continuous large continuous fluctuations to a calm state, it indicates that the rock sample is about to fail.

With the increase of unloading rate, the change of elastic energy and dissipation energy in the post-peak residual

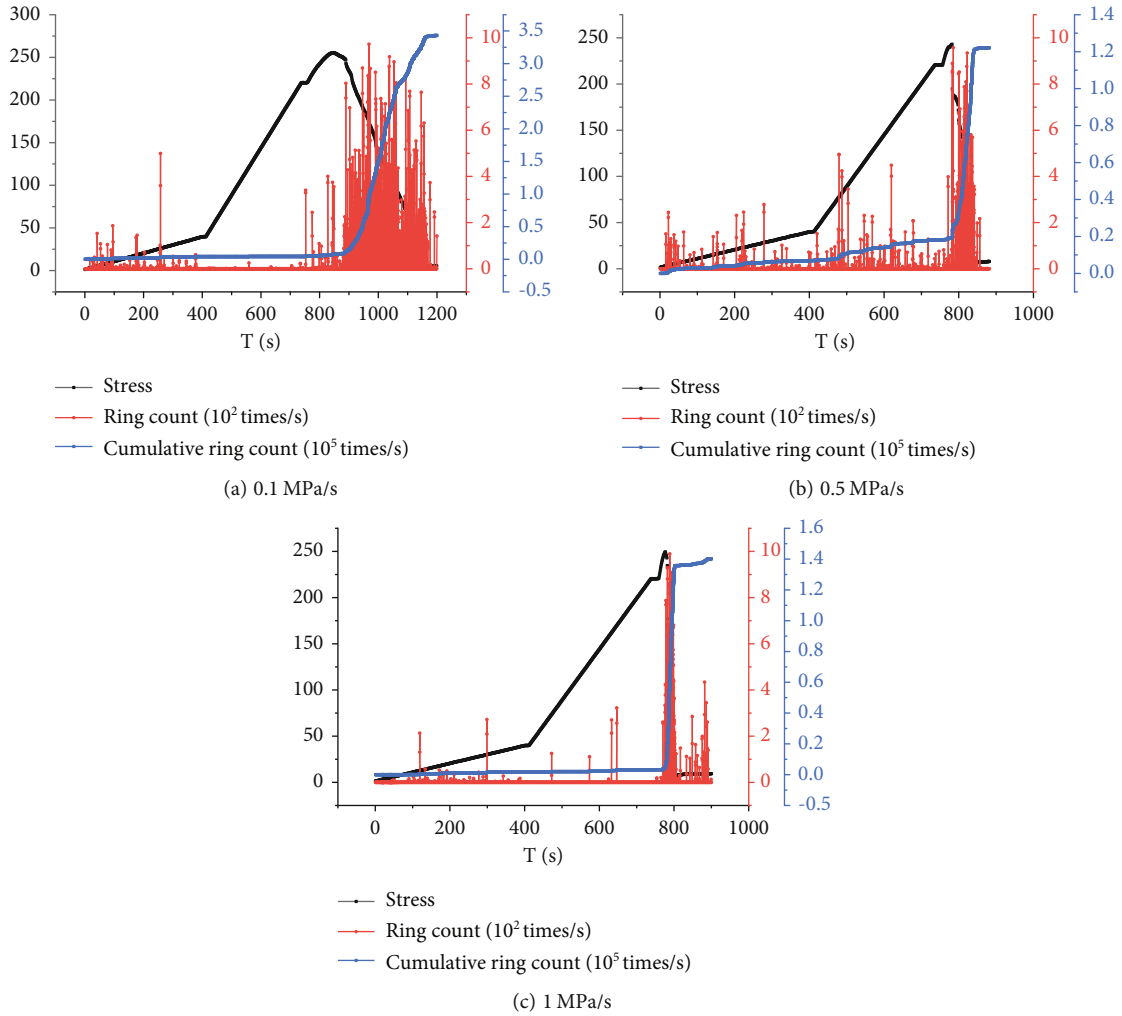

Figure 3: Limestone stress-(cumulative) acoustic emission ringing count-time relationship curve at the same confining pressure with different unloading rates. Note: in the figure, the black vertical coordinate on the left side represents the stress magnitude during the loading of the limestone, the red vertical coordinate on the right side represents the acoustic emission ringing counts during the loading of the limestone, and the blue coordinate represents the cumulative ringing counts.

phase becomes more and more drastic, and the elastic energy plunges, and the dissipation energy rises sharply, indicating that the destruction of rock samples becomes more and more drastic, and the increase of unloading rate can accelerate the destruction of rock samples.

3.2. The Impact of Unloading Rate on Rockburst Damage. Fit the axial strain energy U_1, hoop strain energy U_3, elastic strain energy U_e, dissipation energy U_d, total strain energy U and confining pressure at the peak point, residual point, and unloading point of the rock sample, and the strain energy, and Tables 2–4 show below.

From Figure 2, it can be seen that with the increase of unloading rate, the change of strain energy at each characteristic point is relatively small, which means that the increase of unloading rate has almost the same effect on each strain energy and the sensitivity of strain energy to unloading rate is the same. The acceleration of the destruction of rock samples may be due to that the energy stored before the peak at each unloading rate is the same; that is, the energy released at the residual stage after the peak is the same, and the increase of unloading rate only shortens the destruction time of rock samples and accelerates the release of strain energy but does not change the energy values at the peak and residual points.

In order to intuitively reflect the impact of the unloading rate, the dissipated energy is taken as an example; the time for increasing the dissipation energy from the peak point to the residual point at different unloading rates is listed in Table 5. When the unloading rate is 0.1 MPa/s, the time when the rock sample is loaded to the peak point is 884 s, and the time at the residual point is 1212 s. During this period, it takes 328 s for the dissipated energy to increase. As the unloading rate increases, the time it takes for the dissipated energy to increase is gradually shortened, and the dissipated energy increases. The ground is getting faster and faster, and the rock samples are destroyed more severely.

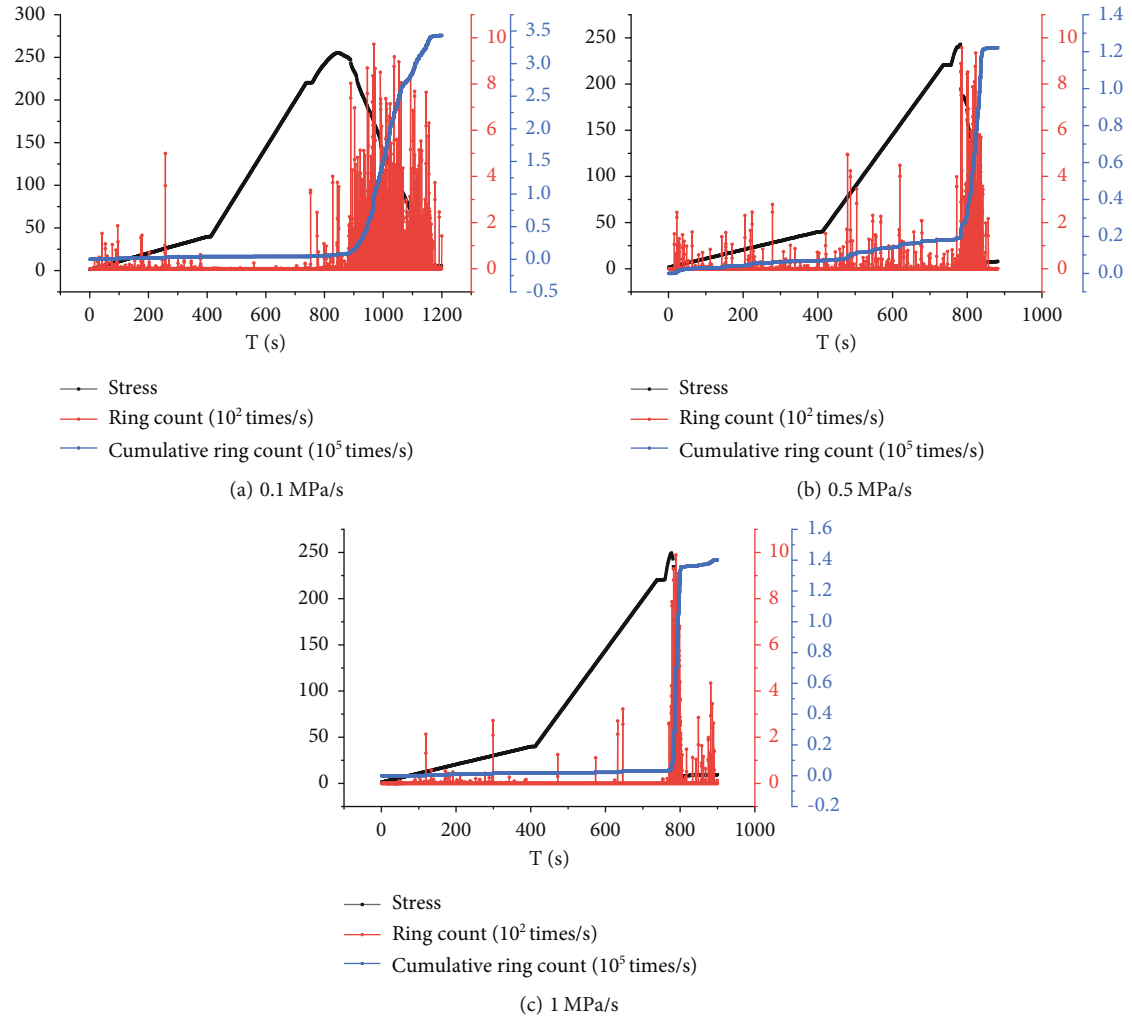

Figure 4: Limestone stress-(cumulative) acoustic emission energy-time relationship curve at the same confining pressure with different unloading rates. Note: in the figure, the black vertical coordinate on the left side represents the stress magnitude during the loading of the limestone, the red vertical coordinate on the right side represents the acoustic emission ringing counts during the loading of the limestone, and the blue coordinate represents the cumulative ringing counts.

Therefore, it can be concluded that in the triaxial compression unloading confining pressure test, after the unloading point, the increase of the unloading rate does not change the energy level of the rock sample at the peak point and the residual point. The impact of loading rate on the rock fracture mainly lies in the following aspects. The time when the sample is loaded to the peak point and the residual point is advanced, and the time when the rock sample ruptures are developed is advanced. The dissipated energy of the rock sample increases faster, and the degree of rock rupture becomes larger.

3.3. Research on Precursory Information of Limestone Unloading Acoustic Emission

3.3.1. Counting Analysis of Acoustic Emission Ringing of Limestone under the Same Confining Pressure and Different Unloading Rates. Acoustic emission parameters can better characterize the changes of rock under external forces, reflecting the internal fine lattice dislocation and crack evolution characteristics in the process of rock material deformation [24, 25]. Among them, the ringing count can reflect the intensity and frequency of the acoustic emission signal [26]. Therefore, the acoustic emission ringing count is selected to analyze the damage of the rock sample during the failure process. Due to the similar trend of unloading rates at 0.1, 0.3, 0.5, 0.7, 1, and 2 MPa/s, the unloading rates of 0.1, 0.5, and 1 MPa/s are selected for analysis due to the limitation of space.

Figure 3 presents the stress-(cumulative) acoustic emission ringing count-time relationship curves of limestones with different unloading rates at the same surrounding pressure (40 MPa). The trend of the (cumulative) ringing count changes at each unloading rate is relatively consistent. Before the rock is loaded to the peak intensity, the ringing count of each specimen is relatively small, with occasional jumps in individual values. The cumulative ringing count curve is relatively flat; this may be due to the fact that the internal

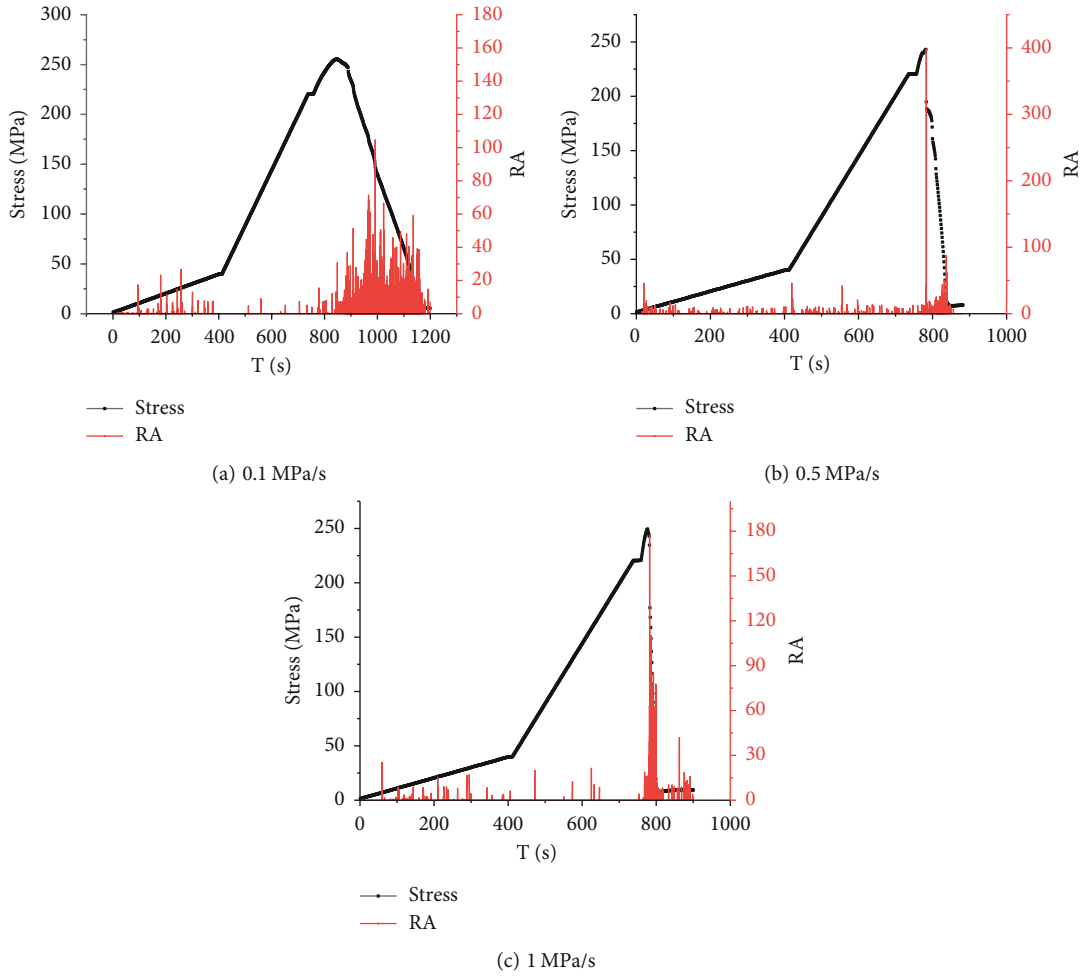

Figure 5: Limestone time-stress-entropy relationship curve under the same confining pressure (40 MPa) and different unloading rates.

fissures of the rock are more developed and produce more acoustic emission signals. When the rock is loaded to the peak intensity, the ringing count program "exploded" and grows to the maximum value within a short period of time, and the accumulated ringing count shows a "vertical rise," indicating that the acoustic emission signal inside the rock is very active at this time. This is because the internal fracture of the rock is fully developed near the peak intensity, which leads to the increase of ringing count.

It can be observed that the change pattern of ringing count near the peak intensity of the rock shows different characteristics at each unloading rate. With the increase of unloading rate, the ringing count near the peak intensity gradually decreases, and the growth trend of cumulative ringing count curve gradually becomes "steeper." When the unloading rate is 0.1 MPa/s, the ringing count is active in 800-1200 s, 0.5 MPa/s ringing count is active in 780-830 s, and when the unloading rate increased to 1 MPa/s, the ringing count is active in 790-820 s, and the ringing count explodes in a very short period of time. This indicates that the increase in unloading rate accelerates the destruction of the rock, resulting in complete destruction of the rock before the acoustic emission signal can be emitted. The increase of unloading rate essentially reflects the increase of unloading volume, and the increase of unloading volume will lead to less restriction on the lateral deformation of the rock, and the rock will be more likely to be destroyed.

The analysis shows that the acoustic emission ringing counts appear intensively and increase "explosively" before the rock sample fractures. The linear increase of the cumulative ringing count indicates that the main fracture of the rock sample is about to occur. As the unloading rate increases, the precursor of rock fracture appears earlier, and the duration becomes shorter and shorter.

3.3.2. Acoustic Emission Energy Analysis of Limestone under the Same Confining Pressure and Different Unloading Rates. When there is external load applied to the rock, the rock will undergo certain deformation. When the applied load exceeds the peak strength of the rock, the internal cracks of the rock will expand through, and then, damage occurs. In this process, energy exchange occurs between the internal and external loads. And the acoustic emission technique can effectively monitor this process, so this subsection studies the process of rock destabilization rupture by observing the acoustic emission energy and the change law of accumulated acoustic emission energy with time and stress.

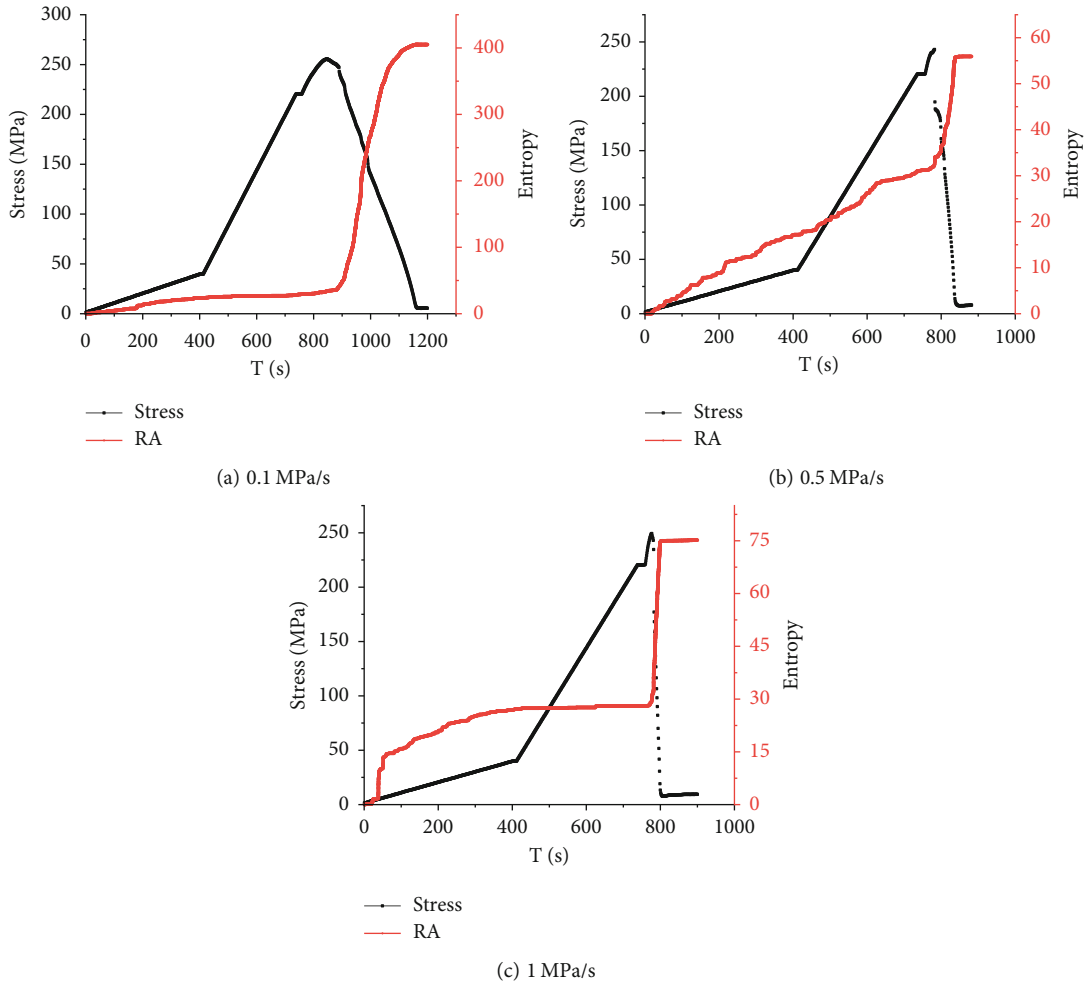

Figure 6: Limestone time-stress-entropy relationship curve under the same confining pressure (40 MPa) and different unloading rates.

Figure 4 shows the relationship curve between stress-(cumulative) acoustic emission energy and time of limestone with different unloading rates at the same confining pressure of 40 MPa. It can be seen that the trends of acoustic emission energy and accumulated acoustic emission energy of rock samples at various unloading rates are basically the same. Loaded in both direction and hoop direction, there are few microcracks inside the rock, and the acoustic emission energy and accumulated energy are almost 0. When the confining pressure reaches the predetermined value, the axial load continues. At this time, the rock is restricted due to the high confining pressure. Limiting the circumferential deformation of the rock. The crack expansion inside the rock is not obvious, resulting in an insignificant energy release with small values and a flat cumulative energy curve. When the axial load reaches 80% of the peak strength of the rock, the confining pressure begins to unload. Due to ring unloading, the ring deformation increases rapidly, and the cracks begin to expand, through, leading to the "explosive" energy growth. The cumulative energy curve shows a "linear" growth, and the rock breaks completely. This change of acoustic emission energy and accumulated energy indicates that the rock is about to fail and rupture. It suggests that the turning point of the curve of energy and cumulative energy from a calm state to a sharp change can be used as the precursor information point of rock rupture.

In order to study the influence of the unloading rate on the precursory information points of rock fracture, the time taken from the beginning of the precursor information point to the end of the precursor phenomenon at each unloading rate for the energy and cumulative energy profiles is counted. Since the energy and cumulative energy curves have the same changing trend, the cumulative energy curve is selected as an example for the ease of description. At 0.1 MPa/s, the cumulative energy curve change interval is 885 s ~1167 s, the time used is 282 s. At 0.5 MPa/s, the cumulative energy curve change interval is 781 s ~848 s; the used time is 67 s. At 1 MPa/s, the cumulative energy curve change interval is 770 s ~810 s; the time used is 40 s. It can be seen that with increasing unloading rate, the occurrence of precursor information points of rock fracture is getting earlier, the time for the cumulative energy curve to grow from a steady state to the maximum value is getting shorter, the slope of the curve is getting larger, and the degree of change is getting more intense.

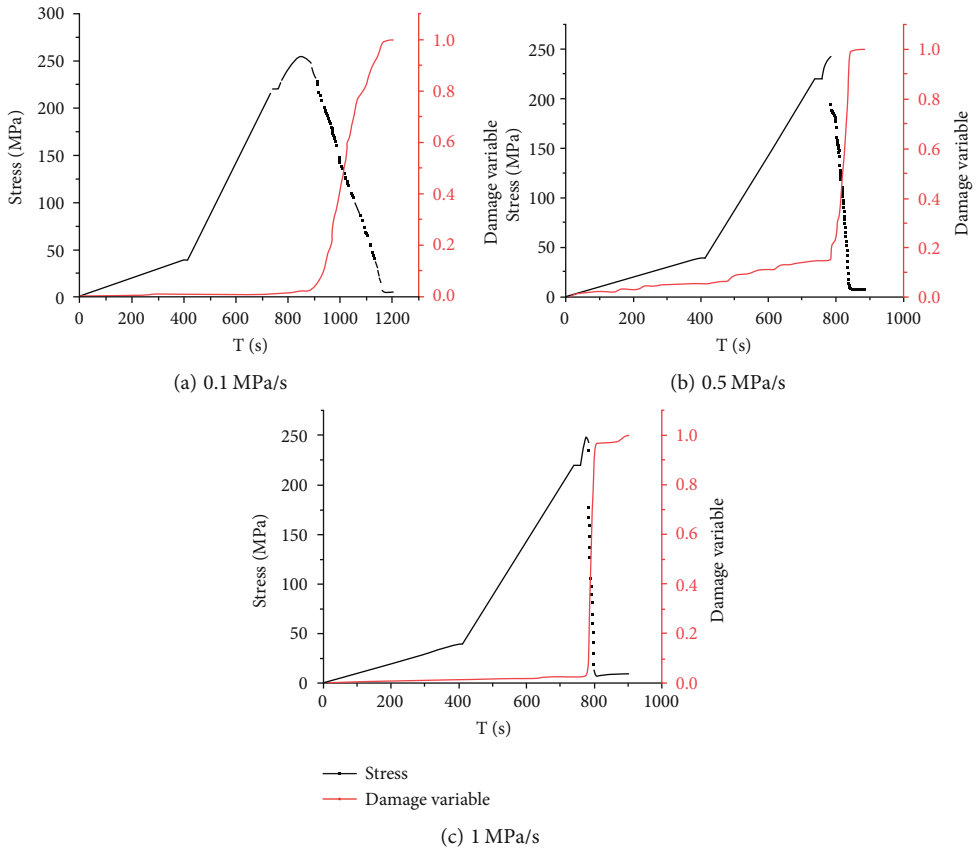

Figure 7: Time-stress-damage variable D relationship curves for limestone under different unloading rates of the same surrounding pressure.

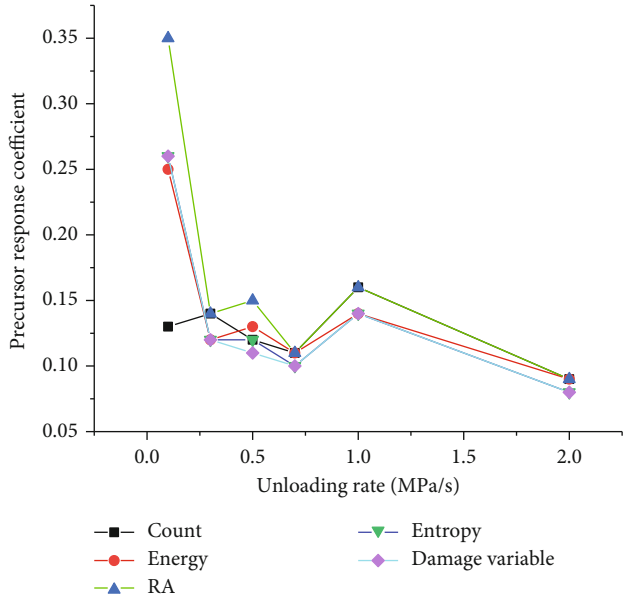

Figure 8: The relationship curve between precursor response coefficient and unloading rate.

3.3.3. Analysis of the RA Value of Limestone Acoustic Emission under the Same Confining Pressure and Different Unloading Rates. RA values of each AE event are calculated based on the rising time and amplitude of each AE waveform, and the variation rule of RA values of limestone during triaxial compression and triaxial loading and unloading failure is analyzed.

Figure 5 shows the time-stress-RA value relationship curve of limestone under the same confining pressure (40 MPa) and different unloading rates. In the early loading stage, the acoustic emission RA value is maintained at a low level, which indicates that the rock sample is mainly composed of shear cracks. As the loading progresses, the internal fissures of the rock sample begin to develop and converge. Around peak stress, the internal fissures of the rock sample have developed sufficiently, and large damages occur. At this time, the RA values begin to appear intensively, and a sudden increase occurs, indicating that a large number of tension cracks are generated at this time. Therefore, the sudden increase in the value of RA near the peak stress can be used as the precursor information of rock fracture.

It is also observed that as the unloading rate increases, the values of rock RA at the peak stress become larger, but the number becomes smaller, and the duration of high RA values is shortened, with RA values of about 100 at 0.1 MPa/s, increasing to about 260 at 1 MPa/s. It is believed that the increase in unloading rate leads to a greater rate of rock destruction, and complete destruction is achieved in a shorter period of time, leading to a reduction of the acoustic emission signal from rock rupture damage. The acceleration of the unloading rate is essentially the increase in the

amount of unloading perimeter pressure. The increase in the unloading volume of the surrounding pressure leads to less restriction on the lateral deformation of the rock, which is more likely to lead to rock damage. It can be concluded that the increase of unloading rate makes the RA value at the information point of rock rupture precursors become larger and shorter in duration.

3.3.4. The Change Law of the Acoustic Emission Entropy Value of Limestone under the Same Confining Pressure and Different Unloading Rates. Figure 6 shows that as the load increases, the acoustic emission entropy grows slowly. At the unloading of confining pressure, entropy increases sharply and reaches the peak value in a relatively short period of time. As a result, the rapid growth of the information entropy of the acoustic emission ringing count before rock failure can be used as a precursor of rockburst.

At the same time, at the stage of rock failure, the entropy increases faster with the increase of unloading rate. At 0.1 MPa/s, the entropy value varies from 883 s to 1124 s in 241 s. At 0.5 MPa/s, the entropy value varies from 771 s to 838 s in 67 s. At 1 MPa/s, the entropy value varies from 771 s to 802 s in 31 s. It can be seen that the higher the unloading rate is, the earlier the turning point of entropy value appears, and the shorter the time to increase to the maximum value is, the more drastic the change of entropy value is. It can be concluded that the effect of unloading rate on precursor of rock failure is mainly as follows: the time of precursor of rock failure is advanced, the duration is shortened, and the variation degree is intensified. For field identification of the rockburst precursor, the effects of unloading rate need to be considered. The increase of unloading rate leads to increasing ringing count entropy change degree, making it easier to capture the precursory characteristics. At the same time, the advance of the entropy timing also makes the precursory characteristics hard to capture.

3.3.5. Acoustic Emission Damage Analysis under the Same Confining Pressure and Different Unloading Rates. Taking 40 MPa confining pressure as an example, the axial strain-axial stress-damage variable curves of the rock sample at various unloading rates are shown in Figure 7. As shown in Figure 7, the growth trend of the damage variable of the rock sample under different unloading rates is roughly the same. Similar to triaxial compression, the change process of the damage variable can also be divided into four stages:

(1) *Damage Formation Stage*. Triaxial unloading stress path is to add unloading confining pressure. The transverse and axial loads are increased at a rate of about 0.1 MPa/s to the target confining pressure value. At this stage, rock is at the elastic stage. Primary cracks are in the initiation and development condition; deformation is not obvious. The damage variable is very small. Rock is at damage formation stage

(2) *Damage Stabilization Stage*. At this stage, confining pressure is preset as 40 MPa and remains unchanged; axial loading rate is 0.5 MPa/s until reaching 80% of rock peak strength. Rock has not yet started unloading the stage and is still in the stage of elastic loading. Native microfracture is not apparent; new crack initiation is less. Damage variable change is very small, from 0.001 to 0.005. It can be understood that the rock is at the "accumulation" stage before unloading failure, and the rock is in the stable stage

(3) *Damage Acceleration Phase*. At this stage, the rock begins to be unloaded. At this time, the axial pressure has reached 80% of the peak strength. The axial pressure continues to be loaded at a loading rate of 0.1 mm/min, and the confining pressure starts to be unloaded from 40 MPa. After unloading, the volume deformation increases rapidly, volume dilatancy is obvious, and lateral strain is also growing at the same time. At this stage, the original cracks continue to develop and expand and converge. New fracture damage variable D value begins to increase. After the peak strength, lateral strain begins to increase, the original crack converges, and macroscopic cracks begin to form, and the damage variable D value shows explosive growth, which is close to the maximum value 1 at the end of unloading. At this stage, rock is at the damage acceleration stage. The explosive growth of damage variable D can be used as precursor information of rock fracture

(4) *Damage and Failure Stage*. At this stage, rock unloading has ended, and rock deformation is still at the residual plastic stage. Rock deformation is still mainly manifested as block slip along the macroscopic fault surface, and the variation trend of damage variables tends to be gentle, and rock is at the postdamage stage

3.4. Multiple Precursor Synthesis Analysis of Acoustic Emission Time Domain Parameters. The above analysis shows that during the loading process, the precursor to identify factors shows relatively consistent laws: (cumulative) acoustic emission ringing count, (cumulative) acoustic emission energy, RA value, acoustic emission information entropy, and acoustic emission damage variables before rock failure becomes active, all show a trend of substantial increase. By analyzing the evolution law of acoustic emission time-frequency signal in the whole process of limestone fracture, it is concluded that the abnormal characteristics of multiple precursor information of acoustic emission time-frequency parameters before rock fracture are as follows: the value increases, and the multiple precursors appear intensively.

In order to facilitate the comparison of the response time sequence of the 5 types of precursor information before limestone fracture, the precursor response coefficients of the above 6 types of signals are, respectively, counted, and the precursor response coefficient calculation formula [27–31]:

$$\sigma = \frac{t_j - t_i}{t_j}, \tag{7}$$

where t_i is the time when the precursor of the acoustic emission indicator appears, t_j is the time when the rock is completely broken. A larger σ indicates the earlier precursory response time of the indicator and the stronger precursory recognition ability.

It can be seen from Figure 8 that the response coefficient of the acoustic emission RA value is still the largest for the same surrounding pressure with different unloading rates, and the identification of rock fracture is the strongest. The response coefficients of the other four indicators fluctuate with the increase of the unloading rate. When the unloading rate is 0.1 MPa/s, the response coefficient of the acoustic emission ringing count is the smallest; the recognition ability is the weakest. The acoustic emission energy, information entropy, and the response coefficient of damage variables are basically the same, and the recognition ability is relatively close. At the unloading rate of 0.5 MPa/s, the response coefficient of acoustic emission energy is the largest, the response coefficient of RA value and information entropy is the second, and the response coefficient of damage variable is the smallest. At other unloading rate, the response coefficients of these four indicators are relatively close, and the ability to identify rock fractures is basically the same.

4. Conclusions

This paper studies the acoustic emission precursor and energy evolution precursor information of limestone under unloading condition, and the research results obtained in this paper are as follows:

(1) The precursory law of rock unloading energy evolution is that the elastic energy decreases rapidly and the dissipated energy increases sharply. During triaxial loading and unloading, the energy pressure drop response ratio changes from large fluctuation state to stable period. These characteristics can be used as precursory information of rock failure. The influence of unloading rate on rock instability failure is discussed, and it is found that with the increase of unloading rate, dissipated energy increases faster, and rock instability failure becomes more serious

(2) Acoustic emission precursor information of rock unloading: the ringing count will increase greatly before rock instability and failure. Acoustic emission energy and accumulated energy will rise rapidly and reach the maximum value before rock instability failure. RA values will appear intensively and start to increase suddenly, and the rock shows tensile failure. The entropy value of ring counting will change from a stable state to a sharp increase, and the slope of the entropy curve will become larger, and the value will increase. Rock changes from damage stability stage to damage acceleration stage, and the damage variable increases rapidly. The variation law of each precursor discriminant index is relatively consistent, and there will be a sudden increase before the rock instability failure. As a result, these information can be used as the precursor information of rock instability failure. The influence of unloading rate on the precursor of rock instability failure is studied, and it is found that the increase of unloading rate will lead to more drastic change of each precursor discrimination index, and each index will complete sudden increase in a short time before rock instability failure

(3) A comprehensive analysis of each precursor discrimination index of acoustic emission was conducted. Based on the precursor response coefficient, the precursor recognition ability was compared. It was found that the RA value response coefficient was the largest, and the precursor recognition ability was the strongest, and the recognition ability of the other four indexes for rock rupture showed fluctuations with the loading path, surrounding pressure and unloading rate. The sudden increase and intensive occurrence of RA value can be taken as the early warning information of rock rupture

Abbreviations

RA: Ratio of risetime to amplitude, risetime/amplitude.

Data Availability

All data included in this study are available upon request by contact with the corresponding author.

Conflicts of Interest

The authors declare that they have no conflicts of interest.

Acknowledgments

This work was financially supported by the National Natural Science Foundation of China (No. 51864023 and No. 51264018).

References

[1] F. Xiating, X. Yaxun, F. Guangliang, Y. Zhibin, and C. Binrui, "Research on the process of rockburst incubation," *Chinese Journal of Rock Mechanics and Engineering*, vol. 38, no. 4, pp. 649–673, 2019.

[2] J. Feifei, Z. Hui, and L. Chang, "Research progress, prediction and prevention of rock burst in underground metal mines," *Chinese Journal of Rock Mechanics and Engineering*, vol. 38, no. 5, pp. 956–972, 2019.

[3] D. Papadopoulos and A. Benardos, "Enhancing machine learning algorithms to assess rock burst phenomena," *Geotechnical and Geological Engineering*, vol. 39, no. 8, pp. 5787–5809, 2021.

[4] J. Zhang, M. Wang, C. Xi et al., "Prediction and evaluation of rockburst based on depth neural network," *Advances in Civil Engineering*, vol. 2021, Article ID 8248443, 11 pages, 2021.

[5] M. He, Z. Zhang, J. Zhu, N. Li, G. Li, and Y. Chen, "Correlation between the rockburst proneness and friction characteristics of rock materials and a new method for rockburst proneness

prediction: field demonstration," *Journal of Petroleum Science and Engineering*, vol. 205, article 108997, 2021.

[6] M. Khan, X. He, A. Farid et al., "A novel geophysical method for fractures mapping and risk zones identification in a coal-mine, Northeast, China," *Energy Reports*, vol. 7, pp. 3785–3804, 2021.

[7] W. Zhang, C. Mu, D. Xu, and Z. Li, "Energy action mechanism of coal and gas outburst induced by rockburst," *Shock and Vibration*, vol. 2021, Article ID 5553914, 14 pages, 2021.

[8] G. Su, G. Zhao, J. Jiang, and X. Hu, "Experimental study on the characteristics of microseismic signals generated during granite rockburst events," *Bulletin of Engineering Geology and the Environment*, vol. 80, no. 8, pp. 6023–6045, 2021.

[9] W. Jing-lin, Y. Wei-li, L. Yi, and S. Couxian, "Rock burst and instability analysis for coal roadways based on unified strength theory," *International Journal of Earth Sciences and Engineering*, vol. 9, no. 5, 2016.

[10] J. Chuanyang, W. Hailong, S. Xizhen, Y. Xianbin, and L. Hengjie, "Study on rockburst prevention technology of isolated working face with thick-hard roof," *Geomechanics and Engineering*, vol. 20, no. 5, 2020.

[11] S. Zhai, G. Su, S. Yin, B. Zhao, and L. Yan, "Rockburst characteristics of several hard brittle rocks: a true triaxial experimental study," *Journal of Rock Mechanics and Geotechnical Engineering*, vol. 12, no. 2, pp. 279–296, 2020.

[12] T. Y. Guo and L. N. Y. Wong, "Cracking mechanisms of a medium-grained granite under mixed-mode I-II loading illuminated by acoustic emission," *International Journal of Rock Mechanics and Mining Sciences*, vol. 145, article 104852, 2021.

[13] T. Qin, Y. Duan, H. Sun, H. Liu, and L. Wang, "Energy evolution and acoustic emission characteristics of sandstone specimens under unloading confining pressure," *Shock and Vibration*, vol. 2019, Article ID 1612576, 9 pages, 2019.

[14] L. Gao, F. Gao, Y. Xing, and Z. Zhang, "An energy preservation index for evaluating the rockburst potential based on energy evolution," *Energies*, vol. 13, no. 14, p. 3636, 2020.

[15] W. Jiaxu, X. Yadong, and G. Yongfa, "Experimental study of time-frequency characteristics of acoustic emission key signals during diorite fracture," *IOP Conference Series: Earth and Environmental Science*, vol. 570, no. 3, article 032054, 2020.

[16] F. Mei, C. Hu, P. Li, and J. Zhang, "Study on main frequency precursor characteristics of acoustic emission from deep buried Dali rock explosion," *Arabian Journal of Geosciences*, vol. 12, no. 21, pp. 1–11, 2019.

[17] C. Wang, C. Cao, Y. Liu, C. Li, G. Li, and H. Lu, "Experimental investigation on synergetic prediction of rockburst using the dominant-frequency entropy of acoustic emission," *Natural Hazards*, vol. 108, no. 3, pp. 3253–3270, 2021.

[18] W. Xinjiang, C. Taotao, and W. Xiao, "Research and progress on rockburst disasters," *Modern Tunnelling Technology*, vol. 57, no. 2, pp. 1–12, 2020.

[19] C. Meifeng, X. Dinglong, and R. Fenhua, "Current status and development strategy of deep mining in metal mines," *Chinese Journal of Engineering Science*, vol. 4, 2019.

[20] Z. Xin, *Research on Rockburst Precursor Information and Rockburst Prediction in Deep Mining*, Kunming University of Science and Technology, 2021.

[21] Q. Shili, F. Xiating, and Z. Chuanqing, "Yang Jinbao experimental research on mechanical properties of deep marble under different initial damage levels and unloading paths," *Chinese Journal of Rock Mechanics and Engineering*, vol. 31, no. 8, pp. 1686–1697, 2012.

[22] C. E. Shannon, "A mathematical theory of communication," *The Bell System Technical Journal*, vol. 27, no. 3, pp. 379–423, 1948.

[23] L. M. Kachanov, "Rupture time under creep conditions," *International Journal of Fracture*, vol. 97, no. 1, 1999.

[24] S. Xue, L. Erbing, D. Jianli et al., "Study on acoustic emission characteristics and damage evolution law of Beishan granite under triaxial compression," *Chinese Journal of Rock Mechanics and Engineering*, vol. 37, no. S2, pp. 4234–4244, 2018.

[25] Y. Zhou, D. Zhao, B. Li, H. Wang, Q. Tang, and Z. Zhang, "Fatigue damage mechanism and deformation behaviour of granite under ultrahigh-frequency cyclic loading conditions," *Rock Mechanics and Rock Engineering*, vol. 54, no. 9, pp. 4723–4739, 2021.

[26] D. Chaofu, L. Jianfeng, C. Liang, L. Yang, and X. Liang, "Fracture mechanical behavior and acoustic emission characteristics of granite with different water-bearing states," *Chinese Journal of Geotechnical Engineering*, vol. 39, no. 8, pp. 1538–1544, 2017.

[27] Z. Yanbo, L. Peng, T. Baozhu, Y. Xulong, S. Lin, and L. Xiangxin, "Multi-parameter coupling analysis of granite catastrophic acoustic emission signals and experimental study on the characteristics of main fracture precursors," *Chinese Journal of Rock Mechanics and Engineering*, vol. 35, no. 11, pp. 2248–2258, 2016.

[28] J. Wang, T. Zuo, X. Li, Z. Tao, and J. Ma, "Study on the fractal characteristics of the pomegranate biotite schist under impact loading," *Geofluids*, vol. 2021, Article ID 1570160, 8 pages, 2021.

[29] Z. Zhang, Q. Qian, H. Wang, Y. Huang, J. Wang, and H. Liu, "Study on the dynamic mechanical properties of metamorphic limestone under impact loading," *Lithosphere*, vol. 2021, no. -Special 4, Article ID 8403502, 2021.

[30] Y. Yang, N. Zhang, and J. Wang, "A study on the dynamic strength deterioration mechanism of frozen red sandstone at low temperatures," *Minerals*, vol. 11, no. 12, p. 1300, 2021.

[31] Y. Yang, N. Zhang, and J. Wang, "Fracture morphology analysis of frozen red sandstone under impact," *Shock and Vibration*, vol. 2021, Article ID 4388132, 12 pages, 2021.